Interface and thickness tuning for blade coated small-molecule organic light-emitting diodes with high power efficiency

Yu-Fan Chang, Yu-Chian Chiu, Hao-Wen Chang, Yi-Siang Wang, Yi-Lun Shih, Chih-Hao Wu, Yi-Lun Liu, Yu-Sheng Lin, Hsin-Fei Meng, Yun Chi, Heh-Lung Huang, Mei-Rurng Tseng, Hao-Wu Lin, Hsiao-Wen Zan, Sheng-Fu Horng, and Jenh-Yih Juang

Citation: Journal of Applied Physics **114**, 123101 (2013); doi: 10.1063/1.4821881
View online: http://dx.doi.org/10.1063/1.4821881
View Table of Contents: http://scitation.aip.org/content/aip/journal/jap/114/12?ver=pdfcov
Published by the AIP Publishing

Interface and thickness tuning for blade coated small-molecule organic light-emitting diodes with high power efficiency

Yu-Fan Chang,[1] Yu-Chian Chiu,[2] Hao-Wen Chang,[3] Yi-Siang Wang,[4] Yi-Lun Shih,[5] Chih-Hao Wu,[3] Yi-Lun Liu,[4] Yu-Sheng Lin,[5] Hsin-Fei Meng,[6,a)] Yun Chi,[7,a)] Heh-Lung Huang,[8] Mei-Rurng Tseng,[8] Hao-Wu Lin,[9,a)] Hsiao-Wen Zan,[1] Sheng-Fu Horng,[3] and Jenh-Yih Juang[2]

[1]*Department of Photonics and the Institute of Electro-Optical Engineering, National Chiao Tung University, Hsinchu 300, Taiwan*
[2]*Department of Electrophysics, National Chiao Tung University, Hsinchu 300, Taiwan*
[3]*Department of Electrical Engineering, National Tsing Hua University, Hsinchu 300, Taiwan*
[4]*Institute of Photonics Technologies, National Tsing Hua University, Hsinchu 300, Taiwan*
[5]*Institute of Imaging and Biomedical Photonics College of Photonics, National Chiao Tung University, Hsinchu 300, Taiwan*
[6]*Institute of Physics, National Chiao Tung University, Hsinchu 300, Taiwan*
[7]*Department of Chemistry, National Tsing Hua University, Hsinchu 300, Taiwan*
[8]*Material and Chemical Research Laboratories, Industrial Technology Research Institute, Hsinchu 310, Taiwan*
[9]*Department of Material Science and Engineering, National Tsing Hua University, Hsinchu 300, Taiwan*

(Received 14 March 2013; accepted 12 August 2013; published online 23 September 2013)

We developed a general method based on fluorescence microscopy to characterize the interface dissolution in multi-layer organic light-emitting diodes (OLEDs) by blade coating. A sharp bi-layer edge was created before blade coating, with the bottom layer being insoluble and top layer soluble. After blade coating, fluorescence images showed that the edge of the top layer shifted when the layer dissolved completely, whereas the bottom layer's edge remained in place as a positioning mark. The dissolution depth was determined to be 15–20 nm when the emissive-layer host of 2,6-bis (3-(9H-carbazol-9-yl)phenyl) pyridine (26DCzPPy) was coated on the hole-transport layer of N,N′-bis(naphthalen-1-yl)-N,N′-bis(phenyl)-benzidine(NPB), which was consistent with a sudden drop in efficiency of orange OLEDs with layer thickness below 20 nm. Thus, the layer thickness of OLEDs was optimized to stay more than 20 nm for blade coating. For a two-color white OLED with the structure TCTA/26DCzPPy:PO-01-TB:FIrpic/TPBI, efficiency was 24 cd/A and 8.5 lm/W at 1000 cd/m^2. For a three-color white OLED with Os(fptz)$_2$(dhpm) added as the emitter, the efficiency was 12.3 cd/A and 3.7 lm/W at 1000 cd/m^2. For a green device with the structure TCTA/26DCzPPy:Ir(mppy)$_3$/TPBI, the efficiency was 41.9 cd/A and 23.4 lm/W at 1000 cd/m^2. © *2013 AIP Publishing LLC*. [http://dx.doi.org/10.1063/1.4821881]

I. INTRODUCTION

Fabricating organic light-emitting diodes (OLEDs) in solution using small molecules is an attractive option because it offers potentially high performance at low cost. Compared to polymers, small molecules have the advantages of a wide range of materials easy purification. Conventionally, vacuum evaporation is used to fabricate small-molecule OLEDs, whereas polymers are fabricated in solution. Depositing small molecules as thin films in solution often suffers from the problems of poor solubility and poor film uniformity because of the weak molecular interactions. For example, spin-coating of small molecules may give disconnected films when the area is large. Because of the problem of inter-layer dissolution, spin-coating is used commonly for a single layer, and the remaining layers are evaporated.[1–4] Blade coating has been used to deposit multi-layers of small molecules without chemical modifications to enhance solubility.[5,6] For phosphorescent OLEDs, good performance was attained with blade coating using small molecules developed originally for vacuum evaporation.[7,8] One of the key features of blade coating is that the dissolution is prevented by drying the wet coated film rapidly by substrate heating and blowing hot air. However, the extent of interface mixing in such a rapid-drying process has not been examined microscopically. With vacuum evaporation, a 5-nm-thick layer can be deposited because interface mixing is absent.[9,10] In blade coating, a small amount of mixing is expected even with the heating, because the underlying solid first layer contacts the solvent of the second layer for approximately two seconds before drying.[6] The lower limit of thickness achieved using current blade-coating methods is a critical factor while optimizing OLED performance by tuning layer thickness.

To study the layer interface microscopically, in this work we developed a general method based on fluorescence imaging of the first layer before and after blade coating of the second layer. Because the first layer lies beneath the second layer after blade coating, conventional surface profiling methods such as atomic force microscopy (AFM) cannot be

[a)]Authors to whom correspondence should be addressed. Electronic addresses: meng@mail.nctu.edu.tw, ychi@mx.nthu.edu.tw, and hwlin@mx.nthu.edu.tw.

used to probe the state of the first layer. A fluorescence microscope can obtain information on the first layer even if it is covered by the second layer, as long as the two layers have distinct emission spectra. In this approach, a sharp edge is created in the first layer before coating, and if the first layer is not dissolved or is only partially dissolved after the blade coating, the edge in fluorescence image will not change. In contrast, if the first layer is complete dissolved, the edge will shift in the direction that the blade moves. As the first layer becomes thinner, the edge starts to shift below a critical thickness, which is identified as the depth of dissolution. This method provides the constraints on tuning layer thickness. The performance of the OLED can then be optimized by varying the concentration and blade speeds to obtain distinct layer thicknesses above the dissolution depth.

Using fluorescence imaging, the extent of interface mixing of a typical hole-transport layer (HTL) was determined to be approximately 15 nm when the common solvent chloroform was used as the solvent for the second layer. This is consistent with the sudden drop in OLED performance when the emission layer is reduced to below 20 nm. When all layer thicknesses were tuned to be more than 20 nm, the optimal white OLED produced using multilayer blade coating gave 24 cd/A and 8.5 lm/W at the practical lighting luminance of 1000 cd/m^2. Only small molecules developed for vacuum evaporation were used in this device. For the green OLED, 41.9 cd/A and 23.4 lm/W were achieved at 1000 cd/m^2. Such high power efficiency makes blade coating of OLEDs a practical technology for lighting.

II. FLUORESCENCE IMAGING OF LAYER DISSOLUTION

Figs. 1(a)–1(d) show the dissolution of the first layer (L_1) after blade coating the second layer (L_2); the layers are examined microscopically to compare the first layer before and after blade coating. Assume that t_1 is the initial thickness of the first layer, and d is the depth of dissolution, given that the first layer is infinitely thick. Fig. 1(b) shows the sharp edge of the first layer created using reactive ion etching (RIE) through a mask. If d is smaller than t_1, the edge of the first layer remains the same, although the layer may become thinner and less uniform because of partial dissolution, as shown in Fig. 1(c). Conversely, if d is larger than t_1, the entire first layer is dissolved. Because the blade moves from the left to right (Fig. 2), the material of the first layer near the sharp edge disappears: it is first removed by the solvent and then re-deposited in regions t_1 on the right side of the edge. As a result, the edge of the first layer, X_1, is shifted toward the right, as shown in Figs. 1(c)–1(e). The shift of the edge of the first layer is measured using a fluorescence microscope that captures fluorescence images of the first layer at selected spectral ranges. The exact position of the first layer before blade coating is registered by adding a layer of poly-(3,4-ethylenedioxythiophene)doped with poly-(styrenesulfonate) (PEDOT:PSS; CLEVIOS^{TM} P VP AI4083) before the first layer, as shown in Fig. 1(a). The PEDOT:PSS layer and L_1 share the same sharp edge created by the same RIE mask. Because PEDOT:PSS is insoluble in most organic

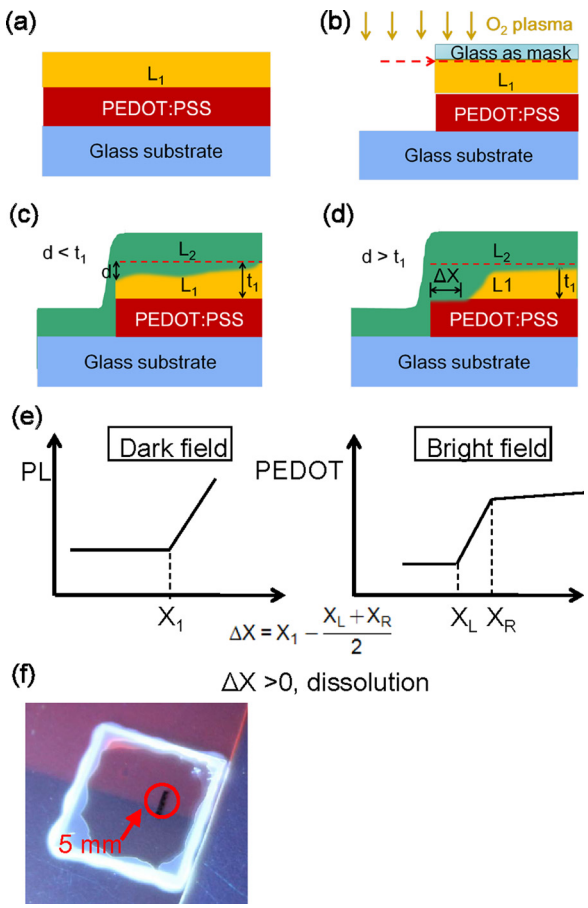

FIG. 1. Schematic diagram for process of observation by fluorescence microscopy. (a) Spin coating PEDOT:PSS and L_1. (b) The clear step made by RIE and the observation interlayer. (c) Expected partial dissolution. (d) Expected dissolution. (e) The image of the definition of ΔX, X_1, X_L, and X_R. (f) The completed bi-layer film etched by RIE is packed with a cover glass.

solvents, blade coating does not affect the PEDOT:PSS edge. After blade coating, bright-field optical microscope images, and dark-field PL image are captured for the same areas. The bright-field images show that the original edge is the edge of both PEDOT:PSS and L_1 before blade coating. The dark-field images show that the edge observed is the L_1 edge after blade coating because PEDOT:PSS is invisible in PL. The difference between the edges in the bright field and

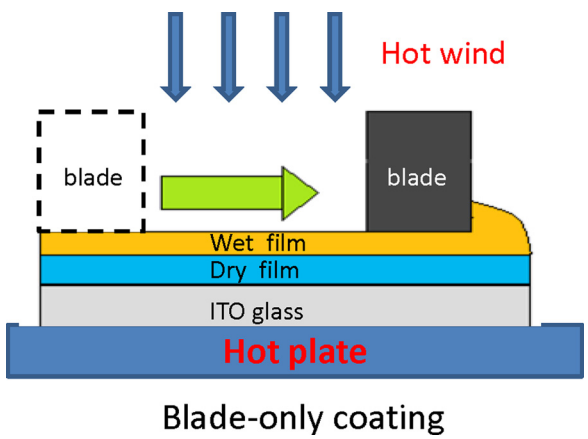

FIG. 2. The blade-only coating process.

PL images is therefore the shift, ΔX. Without using the extra PEDOT:PSS layer to mark positions, the original L_1 edge cannot be located in the PL image after blade coating. When t_1 is below the dissolution depth d, there is a non-zero shift in ΔX, meaning that X_1 is on the right of the PEDOT:PSS edge. When t_1 is above d, the edge does not shift, meaning that X_1 lies at the PEDOT:PSS edge. The position of d can be determined by measuring the shift using L_1 with various t_1 thicknesses. The edge is shifted when t_1 is less than a specified critical thickness, which is then taken as the dissolution depth.

An Olympus fluorescence microscope with a mercury light source was used. The excitation band of 360–370 nm was chosen using a filter. When the L_1 layer was poly(N-vinylcarbazole) (PVK) doped with a red dye, a long wave pass band-pass filter for 480 nm was used to capture the fluorescence image, and when N,N′-bis(naphthalen-1-yl)-N,N′-bis(phenyl)-benzidine (NPB) was added to the L_1 layer, a short wave pass filter for 492 nm was used to select the blue fluorescence. The emission spectra of the materials used and the band selections are presented in Fig. 3, and chemical structures of the materials are presented in Fig. 4.

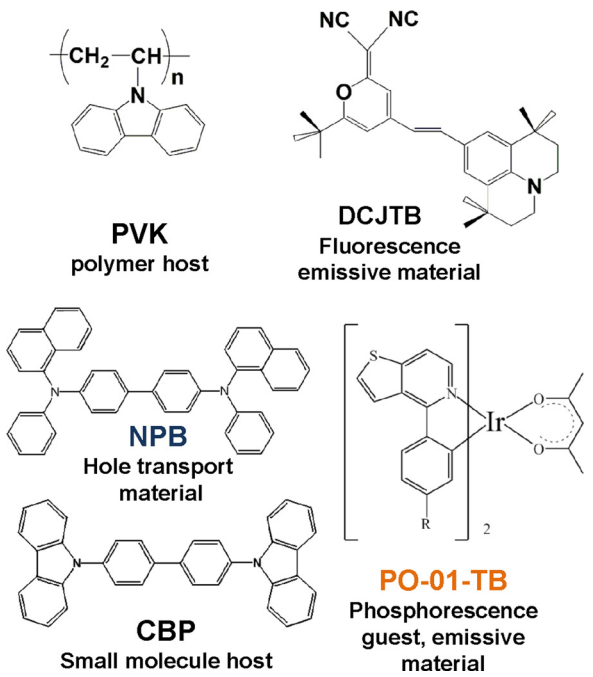

FIG. 4. The chemical structures are used in the dissolution study.

A. Dissolution of PVK doped with red dye

As a proof of concept for the method developed here to measure dissolution, two L_1 layers with distinct solubilities were compared. The first PVK sample has a low molecular weight (12 k) and was doped with the red dye DCJTB (4-(dicyanomethylene)-2-tert-butyl-6-(1,1,7,7-tetramethyljulolidin-4-yl-vinyl)-4H-pyran) for fluorescence imaging; pure chloroform was used as the solvent for blade coating. The second sample was PVK with a high molecular weight of 1.1 million, which was doped with DCJTB, and blade coating was with saturated methanol solution of 2,2′,2″-(1,3,5-benzinetriyl)-tris (1-phenyl-1-H-benzimidazole) (TPBI). TPBI saturation was performed to reduce the solubility of methanol. The first and second cases are therefore examples of high and low dissolution, respectively. However, these are not typical layers of OLEDs, but simple examples to illustrate the concept; regular OLED bilayers are described below.

A 40-nm layer of PEDOT:PSS was spin-coated at 2000 rpm on indium-tin oxide (ITO) glass and then annealed at 200 °C for 15 min in air. L_1 was a blend of PVK and DCJTB in the weight ratio of 94:6. The blend in chloroform (0.2 wt. %) was blade coated with a gap of 60 μm, spun at 2000 rpm, and then annealed at 100 °C for 10 min in vacuum. After completing the PEDOT:PSS and L_1 layers, we used the RIE system at 100 W for 3 min to etch the bilayer film. The completed bilayer film etched by RIE was packed with a cover glass, as shown in Fig. 1(f), to prevent photo-oxidation during PL microscopic imaging. The red color in images shows the PVK:DCJTB film, and the black line across the RIE edge is marked as a guide for microscopy. The bright-field and fluorescence images for PEDOT:PSS/PVK:DCJTB (L_1) with the 12-k molecular weight PVK are shown in Fig. 5 before and after blade coating with pure chloroform. Before blade coating, the red PL edge $X_1 = 834$ μm of L_1 lay between the boundaries $X_L = 824$ μm and $X_R = 842$ μm of

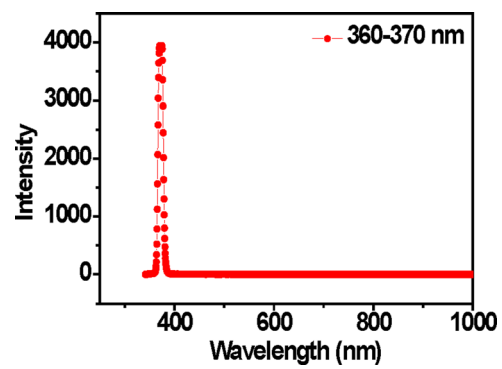

FIG. 3. The emission spectra of the involved materials and the band selections.

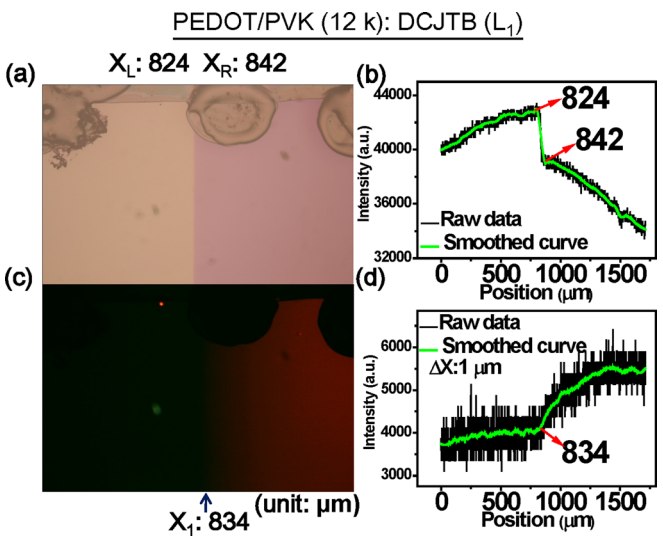

FIG. 5. (a), (b) The bright-field, (c) (d) the dark-field plus fluorescence images of PEDOT/12 K PVK:DCJTB (L_1).

the PEDOT edge in the numerical grey-level profile across the bright-field image as expected, because both PEDOT and L_1 were etched using the RIE mask shown in Fig. 1(b). The coordinates X_1, X_L, and X_R are in micrometers. After chloroform coating, the PL edge shifted to the right of the range, as shown in Fig. 6, demonstrating that X_1 was larger than X_R and indicating that L_1 was dissolved completely by the chloroform blade coating. To confirm that the PL shift meant that L_1 was dissolved, we used independent methods; Figs. 7–9 show fluorescence and AFM images as results of two independent tests. In the PL image, the red fluorescence appears uniform before the chloroform blade coating. After blade coating, red dots are seen away from the edge (Fig. 8). The average size was approximately 20 μm. This probably reflects the poor uniformity of the PVK:DCJTB mixture, first dissolved and then re-deposited on the PEDOT surface. The change in surface morphology was also studied using AFM before after blade coating. The roughness was only 0.7 nm before coating. After coating, a dot was seen in the AFM image, and including the dot the roughness rose to 6.5 nm; even in regions without the dot, roughness increased to 2.6 nm. Additionally, polygonal patterns appeared after blade coating. The formation of large dots and the distinct surface morphology suggest that the 12-k PVK was dissolved effectively. The results of PL shift, the wide range of PL images, and AFM images indicated strong dissolution of PVK consistently.

Now we turn to the example of PVK with a high molecular weight of 1.1 million. Figs. 10 and 11 show that the PL edge did not shift after blade coating with the methanol:TPBI solution: the edge X_1 lies between X_R and X_L before and after the coating, indicating weak dissolution. Fluorescence imaging and AFM were used to confirm the dissolution of the high molecular weight PVK. Figs. 12 and 13 show no red dots, presumably because of weak dissolution and re-deposition. AFM imaging (Fig. 14) also showed similar roughness and stripe patterns before and after methanol:TPBI coating. The roughness may be increased slightly because of the deposition of a thin TPBI layer. These two studies using PVK with high and low molecular weights demonstrate that the shift of the PL image away from its original edge can be used as an evidence of dissolution of L_1 layer caused by the blade coating. In the multilayer OLED structure, L_1 lies underneath L_2 after coating, and therefore AFM cannot be used to characterize L_1. PL imaging therefore becomes a useful method to study the layer's state near the edge even when it is buried under L_2.

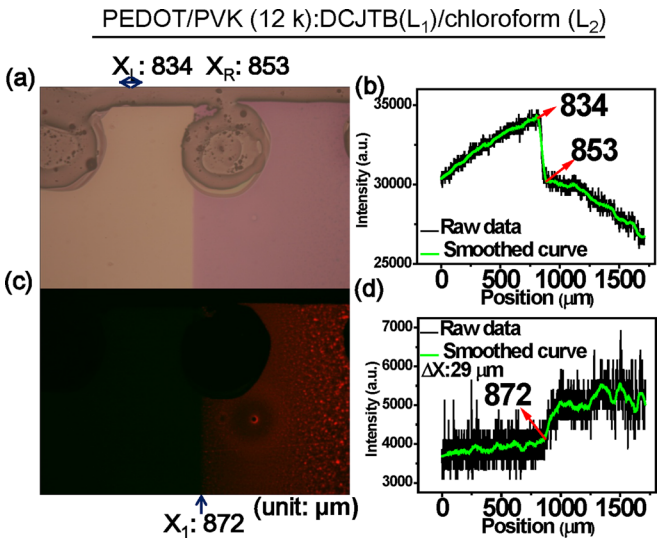

FIG. 6. (a), (b) The bright-field, (c), (d) the dark-field plus fluorescence images of the PL edge shift to the right.

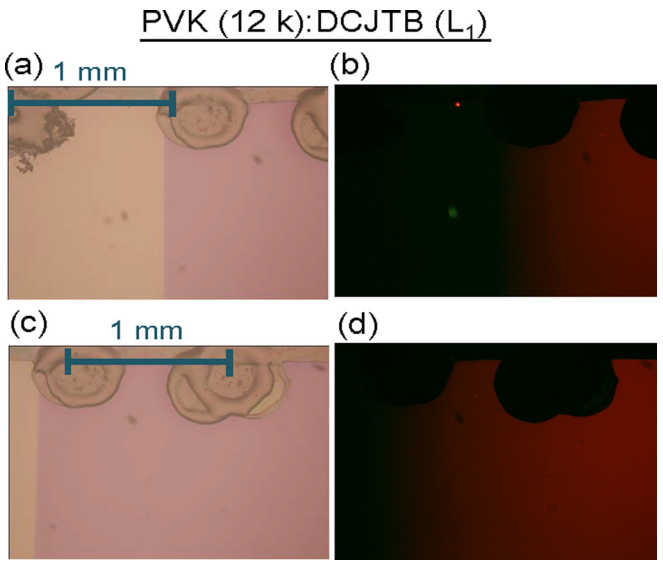

FIG. 7. (a), (b) The bright-field, (c), (d) the dark-field of the wide range fluorescence image of PEDOT:PSS/12 K PVK:DCJTB (L_1).

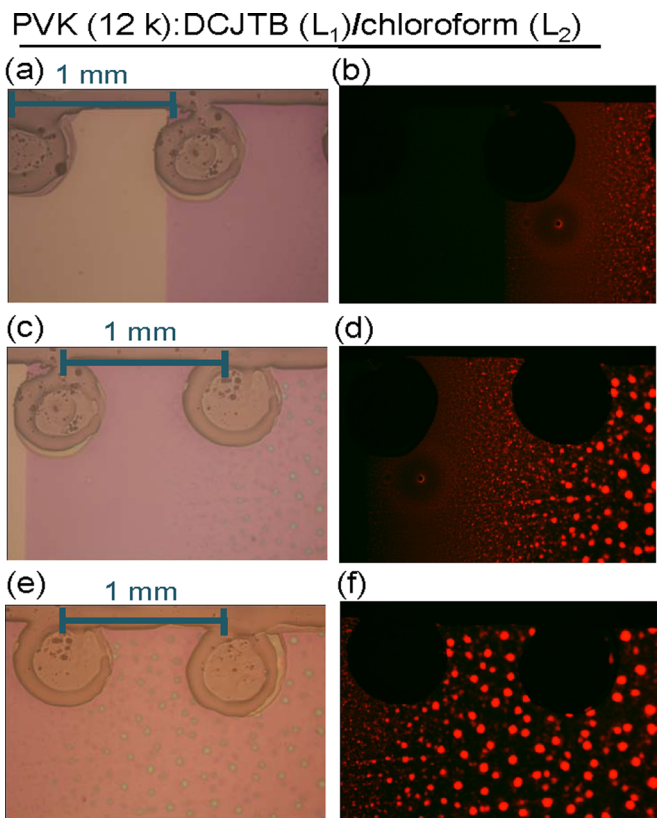

FIG. 8. (a), (b) The bright-field, (c), (d) the dark-field of the wide range fluorescence image of 12 K PVK:DCJTB (L_1)/chloroform (L_2) with the PL edge shift to the right of the range.

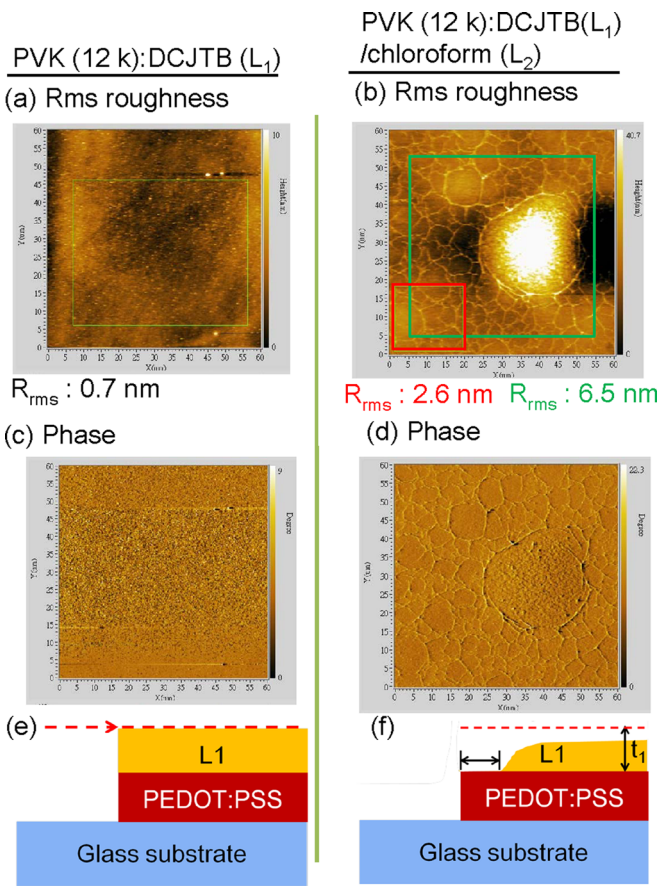

FIG. 9. The AFM images of 12 K PVK:DCJTB (L_1) (a) rms roughness and (c) phase. The AFM images of 12 K PVK:DCJTB (L_1)/chloroform (L_2) (b) rms roughness and (d) phase. The profile images of (e) 12 K PVK:DCJTB(L_1) and (f) 12 K PVK:DCJTB (L_1)/chloroform (L_2).

B. Dissolution of NPB hole-transport layer

1. Changing L1 thickness for chloroform coating

The method discussed above was applied to the regular bilayer structures of OLEDs, including the HTL NPB as L_1 and the phosphorescent emissive layer of 4,4′-bis(carbazol-9-yl) biphenyl (CBP):PO-01-TB as L_2. The chemical structures of these materials are presented in Fig. 4. A 50-nm layer of PEDOT:PSS was spin-coated at 2000 rpm on ITO glass and annealed at 200 °C for 15 min in air. NPB was dissolved in toluene at 0.2 wt. %, 0.3 wt. %, 0.4 wt. %, and 0.5 wt. %, and then blade coated with a gap of 60 μm; 30 μl of the solution was delivered using a pipette to the sample on a hot plate at 60 °C and then annealed at 120 °C for 5 min in vacuum, which generated solid films of thickness 15 nm, 20 nm, 30 nm, and 35 nm. The standard condition was PEDOT:PSS/35 nm NPB (Fig. 15). After completing the PEDOT:PSS layer and L_1, we used the RIE system at 100 W for 3 min to etch the bilayer film. We measured the dissolution of the L_1/L_2 bilayer structure in which L_1 was NPB with varying thicknesses t_1, and L_2 was blade coated with

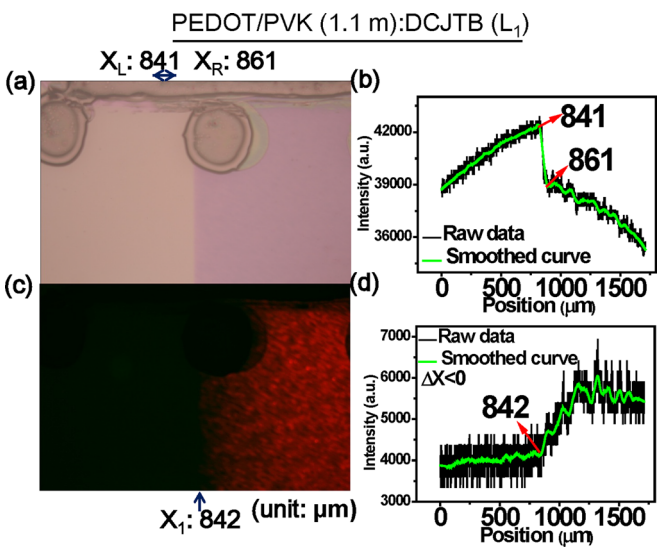

FIG. 10. (a), (b) The bright-field, (c) (d) the dark-field plus fluorescence images of PEDOT:PSS/1.1 million PVK:DCJTB (L_1).

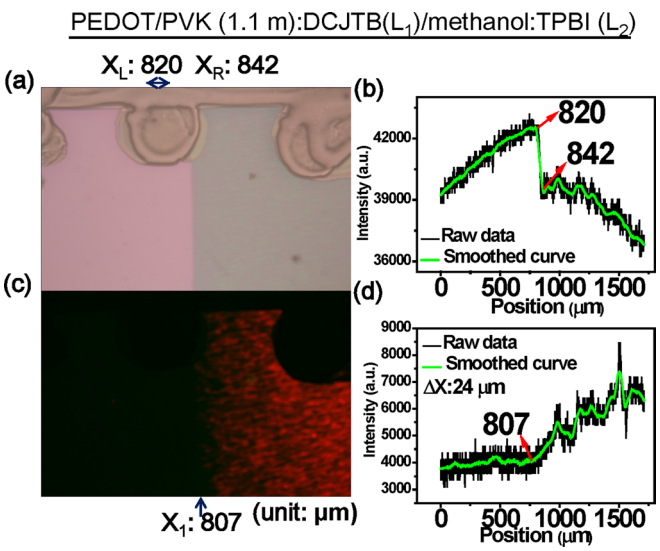

FIG. 11. (a), (b) The bright-field, (c), (d) the dark-field of the fluorescence image of 1.1 million PVK:DCJTB (L_1)/methanol:TPBI (L_2) with the PL edge shift to the right.

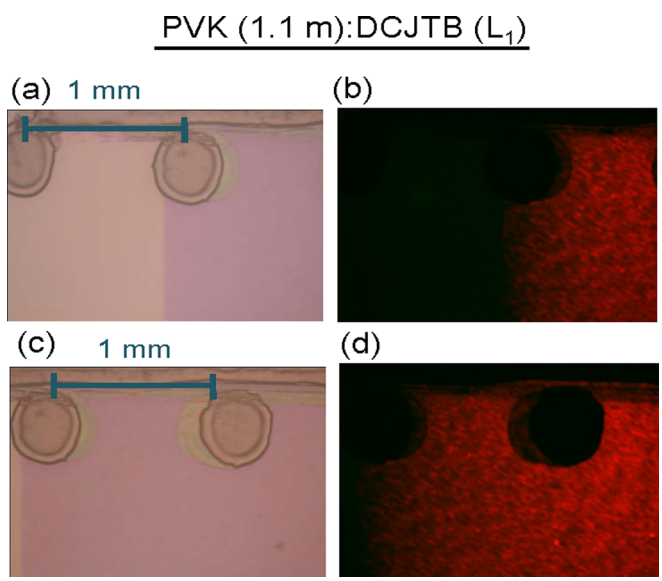

FIG. 12. (a), (b) The bright-field, (c), (d) the dark-field of the wide range fluorescence image of PEDOT:PSS/1.1 million PVK:DCJTB (L_1).

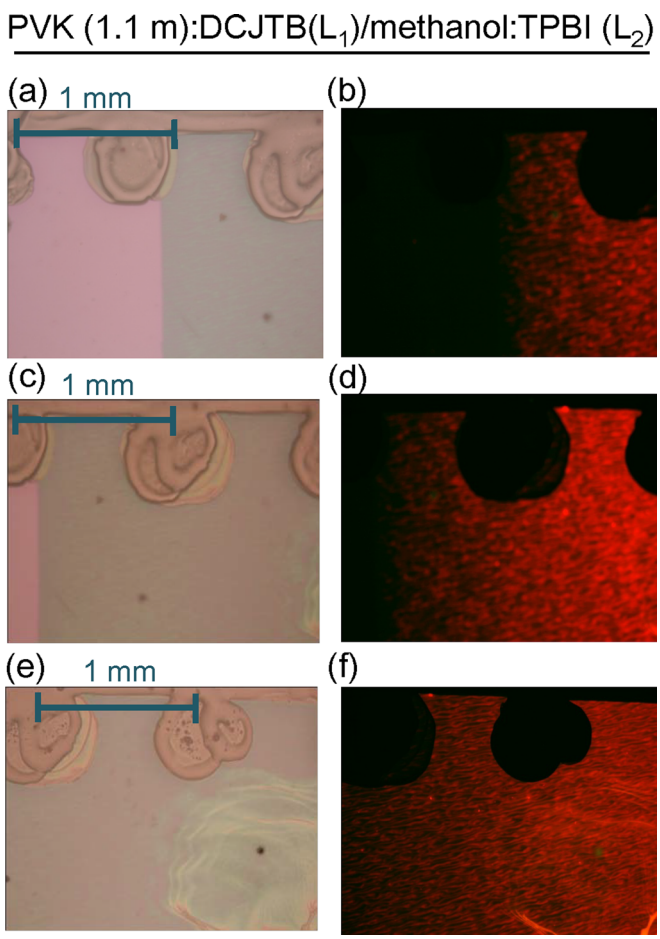

FIG. 13. (a), (c), (e) The bright-field, (b), (d), (e) the dark-field of the wide range fluorescence image of 1.1 million PVK:DCJTB (L_1)/methanol:TPBI (L_2) with the PL edge shift to the right.

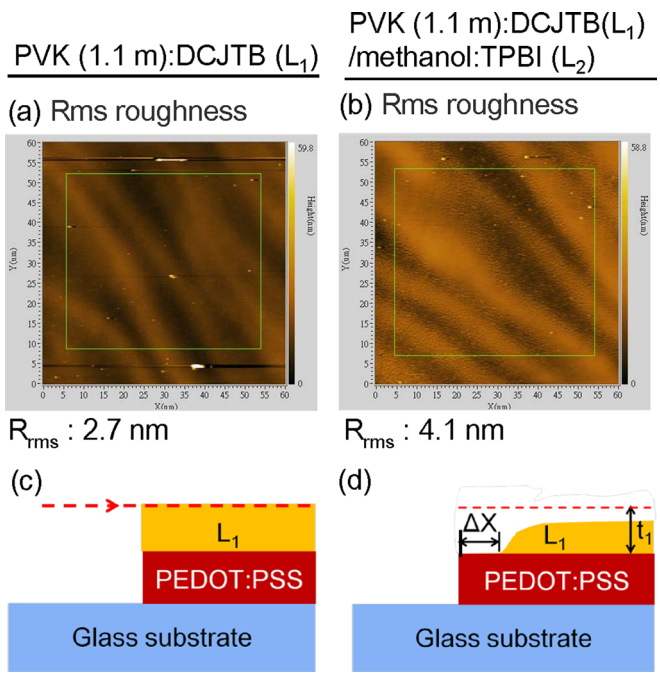

FIG. 14. The AFM rms roughness images of (a) 1.1 million PVK:DCJTB (L_1) and (b) 1.1 million PVK:DCJTB (L_1)/methanol:TPBI (L_2). The profile images of (c) 1.1 million PVK:DCJTB (L_1) and (d) 1.1 million PVK:DCJTB (L_1)/methanol:TPBI (L_2).

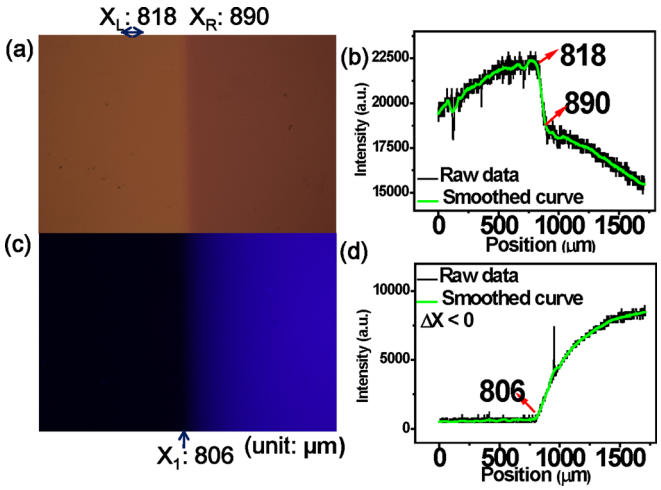

FIG. 15. (a), (b) The bright-field, (c), (d) the dark-field of the standard condition is PEDOT:PSS/35 nm NPB.

CBP:PO-01-TB dissolved in chloroform at 0.5 wt. %. The sharp edge of PEDOT:PSS lies between its left and right boundaries X_L and X_R, shown near the sudden jump in the numerical grey level for the bright field image in Fig. 1(e). The edge of L_1 before L_2 blade coating also lies between X_L and X_R, although this edge is not visible in the bright field image because NPB is transparent. Fig. 15 shows the PL image of L_2 before blade coating, and the edge X_1 of L_1 lies between X_R and X_L as expected. After L_2 blade coating, the original edge of L_1 is no longer visible in the PL image but should still be between X_R and X_L. If L_1 dissolves only partially (i.e., $d < t_1$), after L_2 blade coating the edge X_1 of NPB PL should still lie between X_L and X_R, which was the case for L_1 thicknesses of 20 nm, 30 nm, and 35 nm (Figs. 16–18). These results demonstrate that for the strong solvent chloroform, the depth of dissolution d was below 20 nm with rapid drying of substrate by heating and blowing hot air. In contrast, for the L_1 thickness of 15 nm shown in Fig. 19, the PL edge shifted out of the range of the original edge, meaning that X_1 became larger than X_R. This indicates that the entire L_1 film was dissolved by the solvent of L_2 blade coating, and

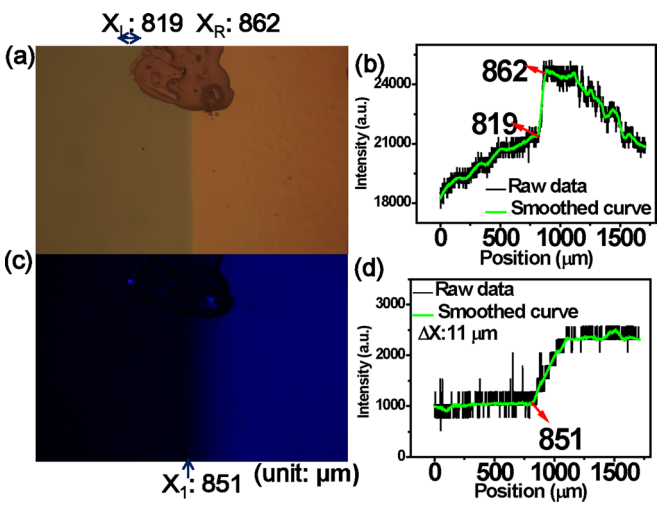

FIG. 16. (a), (b) The bright-field, (c), (d) the dark-field of the structure condition is PEDOT:PSS/20 nm NPB/CBP:PO-01-TB with chloroform solvent.

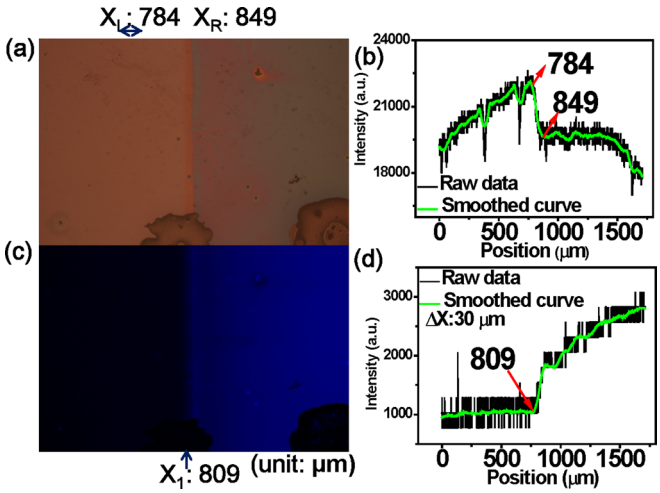

FIG. 17. (a), (b) The bright-field, (c), (d) the dark-field of the structure condition is PEDOT:PSS/30 nm NPB/CBP:PO-01-TB with chloroform solvent.

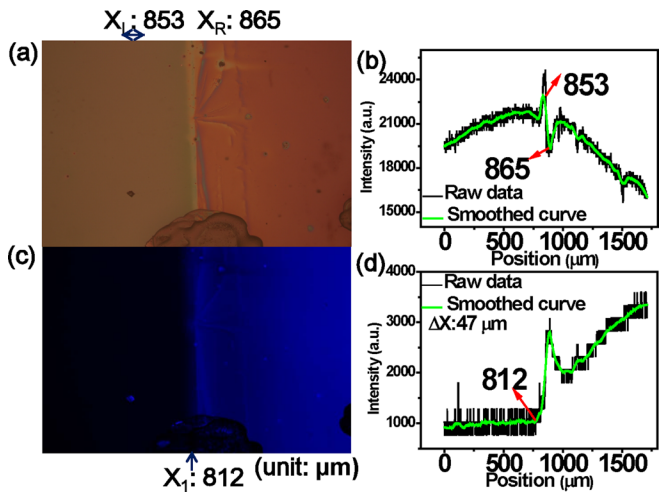

FIG. 18. (a), (b) The bright-field, (c), (d) the dark-field of the structure condition is PEDOT:PSS/35 nm NPB/CBP:PO-01-TB with chloroform solvent.

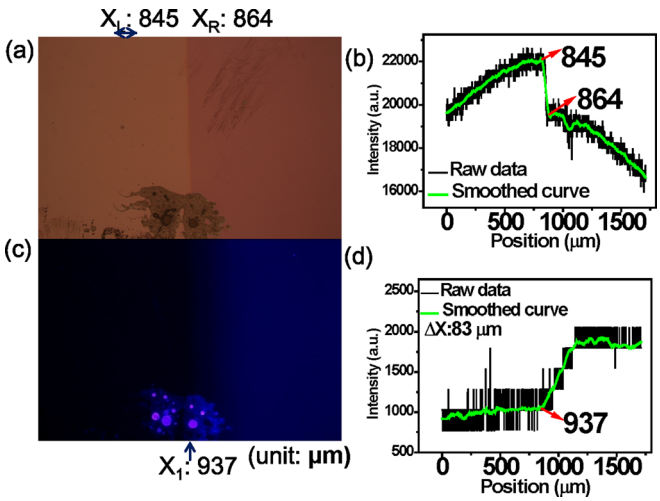

FIG. 19. (a), (b) The bright-field, (c), (d) the dark-field of the structure condition is PEDOT:PSS/15 nm NPB/CBP:PO-01-TB with chloroform solvent.

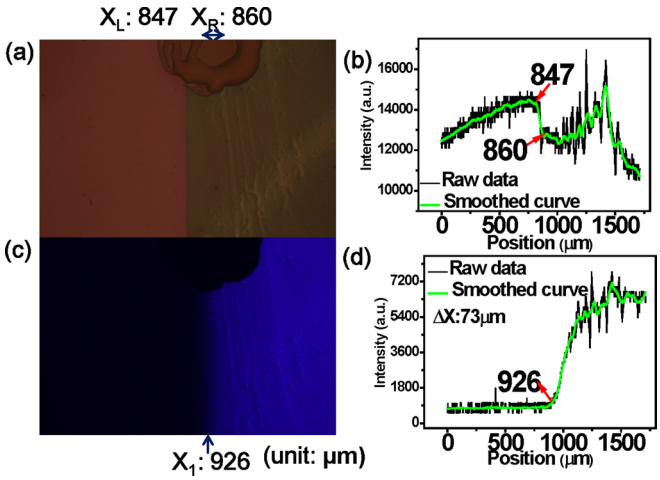

FIG. 20. (a), (b) The bright-field, (c), (d) the dark-field of the structure condition is PEDOT:PSS/15 nm NPB/CBP:PO-01-TB with toluene solvent.

therefore the NPB was pushed toward the right as the blade moved in that direction. The dissolution depth was thus greater than 15 nm. Based on the results obtained with all thicknesses, we conclude that the dissolution depth d is between 15 nm and 20 nm for chloroform. Given the current blade-coating conditions, a clean layer below 20 nm cannot be deposited because of dissolution, but layers above 30 nm can be deposited reliably with only minor dissolution. Next, we changed the solvents for L_2 coating to toluene and chlorobenzene and observed that the L_1 thickness was 35 nm (Figs. 20–27) and that the PL edge shifted out of the range of the original edge (Table I). The dissolution depth was therefore more than 35 nm for these two solvents.

2. Changing coating solvent for a fixed L_1 thickness of 20 nm

Next, we studied the dissolution of L_1 with a fixed thickness of 20 nm when solvents for L_2 were changed to include toluene, chloroform, and chlorobenzene. Pure methanol was also blade coated as a reference, because the

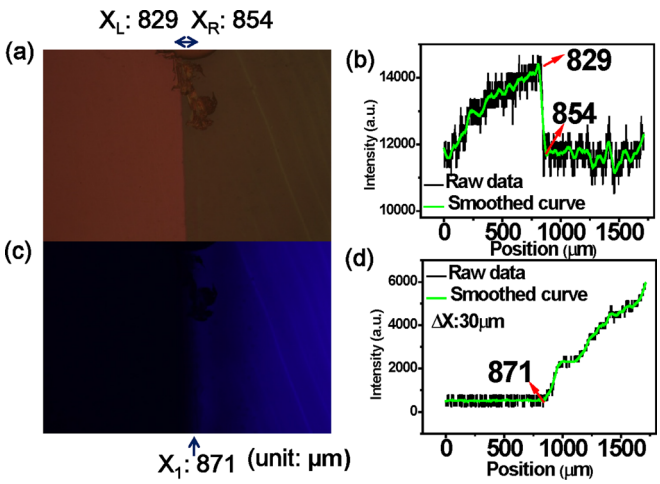

FIG. 21. (a), (b) The bright-field, (c), (d) the dark-field of the structure condition is PEDOT:PSS/20 nm NPB/CBP:PO-01-TB with toluene solvent.

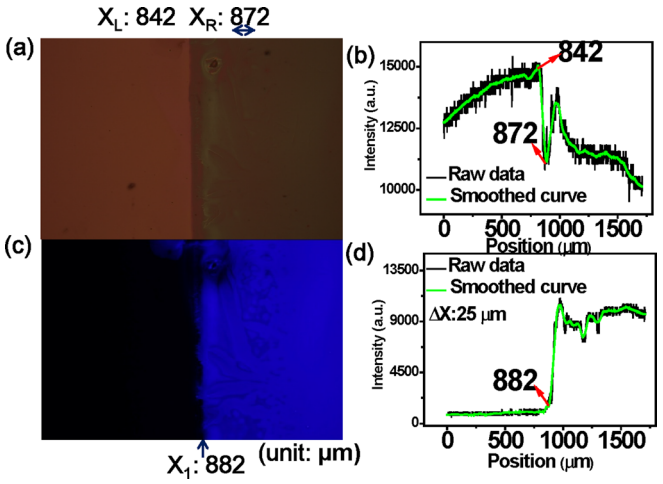

FIG. 22. (a), (b) The bright-field, (c), (d) the dark-field of the structure condition is PEDOT:PSS/30 nm NPB/CBP:PO-01-TB with toluene solvent.

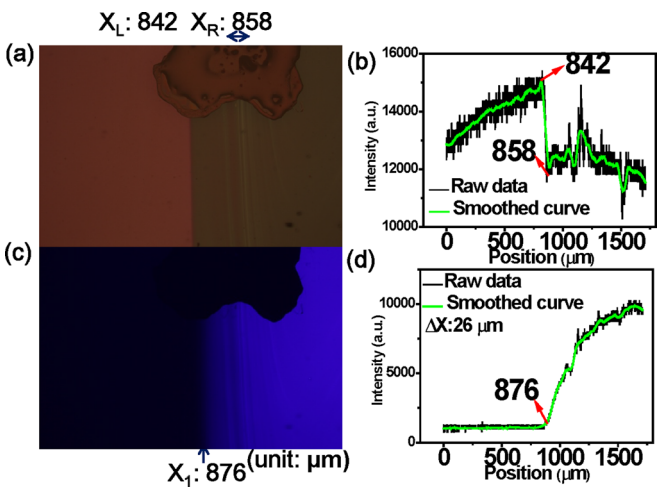

FIG. 23. (a), (b) The bright-field, (c), (d) the dark-field of the structure condition is PEDOT:PSS/35 nm NPB/CBP:PO-01-TB with toluene solvent.

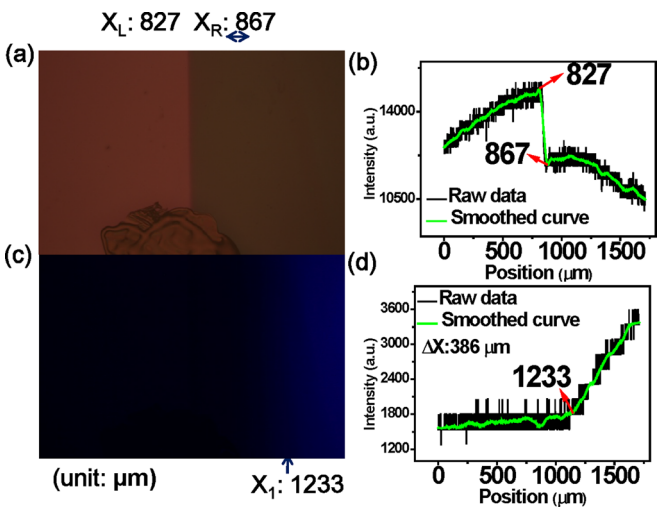

FIG. 24. (a), (b) The bright-field, (c), (d) the dark-field of the structure condition is PEDOT:PSS/15 nm NPB/CBP:PO-01-TB with chlorobenzene solvent.

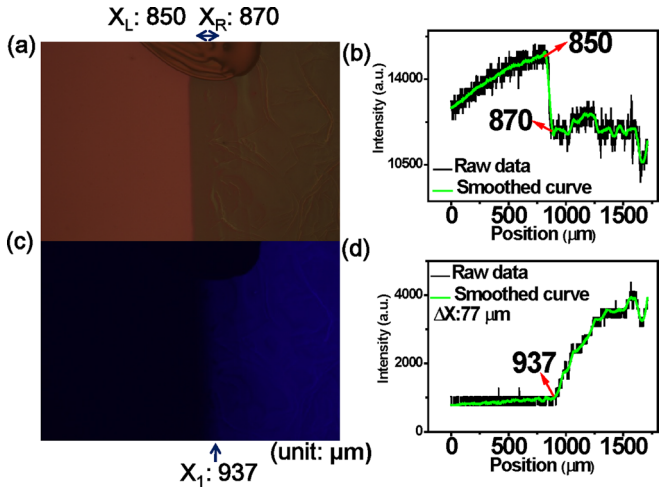

FIG. 25. (a), (b) The bright-field, (c), (d) the dark-field of the structure condition is PEDOT:PSS/20 nm NPB/CBP:PO-01-TB with chlorobenzene solvent.

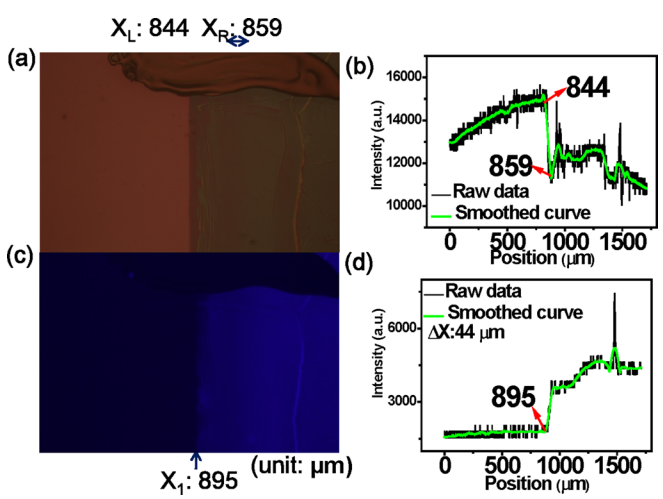

FIG. 26. (a), (b) The bright-field, (c), (d) the dark-field of the structure condition is PEDOT:PSS/30 nm NPB/CBP:PO-01-TB with chlorobenzene solvent.

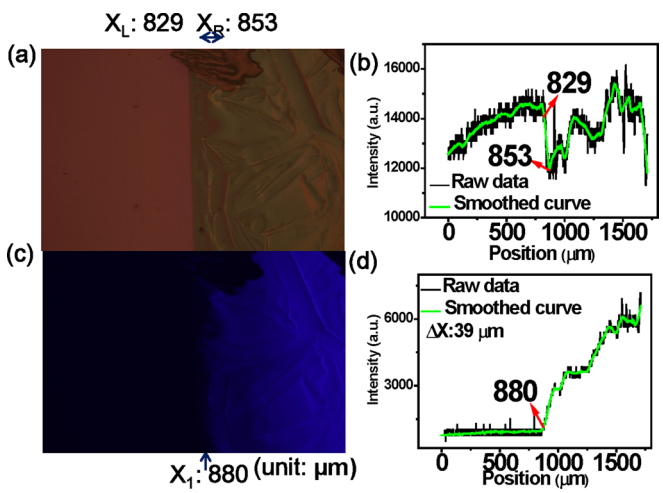

FIG. 27. (a), (b) The bright-field, (c), (d) the dark-field of the structure condition is PEDOT:PSS/35 nm NPB/CBP:PO-01-TB with chlorobenzene solvent.

TABLE I. The degree of dissolution with different solvent and HTL thickness.

Solvent	HTL thickness (nm)	ΔX (μm)
Chloroform	15	83
Chloroform	20	11
Chloroform	30	30
Chloroform	35	47
Toluene	15	73
Toluene	20	30
Toluene	30	25
Toluene	35	26
Chlorobenzene	15	386
Chlorobenzene	20	77
Chlorobenzene	30	44
Chlorobenzene	35	39

L_1 of NPB in almost insoluble in methanol. After methanol coating, the L_1 edge X_1 was still between the original edge ranges of X_L and X_R as expected (Fig. 28). For other solvents, L_1 was composed of NPB as before. The L_1 edge did not shift, as shown in Figs. 29 and 30, and $X_L < X_1 < X_R$ for toluene and chloroform, meaning that the dissolution depth d for the two solvents was below 20 nm, agreeing with the previous chloroform results. Because toluene is a considerably weaker solvent than chloroform, a dissolution depth below 20 nm was expected, and toluene would be suitable for multilayer blade coating if this dissolution were the only consideration. However, toluene poorly dissolves certain small molecules used for the L_2 layer, and hence its application is limited. The result for chlorobenzene showed a clear shift of the PL edge out of the original range (Fig. 31). The dissolution depth of chlorobenzene was therefore higher than 20 nm. Among all the solvents tested above, chlorobenzene is the only one that dissolved to more than 20 nm despite substrate heating and the use of hot air (Table II). Because chlorobenzene boils at a much higher temperature (131 °C) than chloroform (61.2 °C), chlorobenzene dries considerably slower than chloroform given the

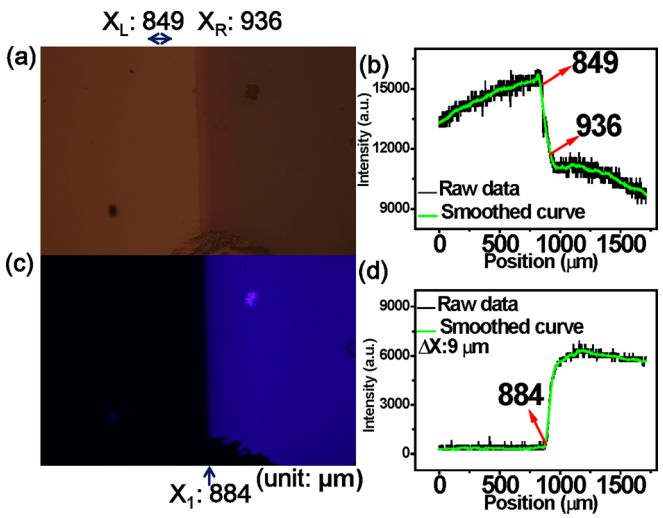

FIG. 28. (a), (b) The bright-field, (c), (d) the dark-field of fixing the thickness of NPB and using pure methanol with heating and hot-wind.

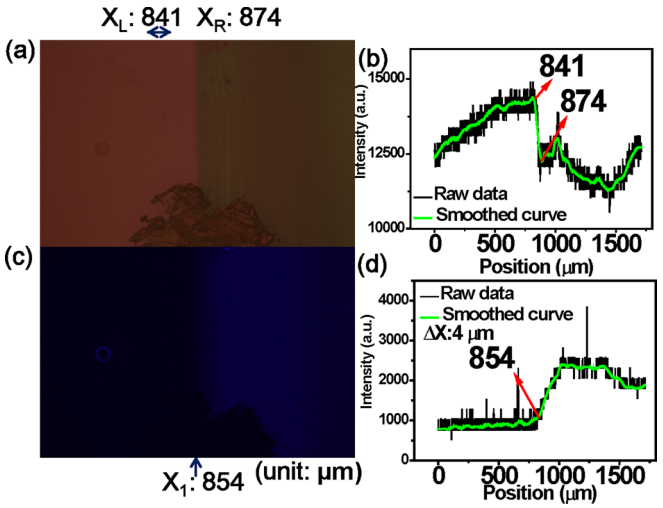

FIG. 29. (a), (b) The bright-field, (c), (d) the dark-field of fixing the thickness of NPB and using toluene solvent with heating and hot-wind.

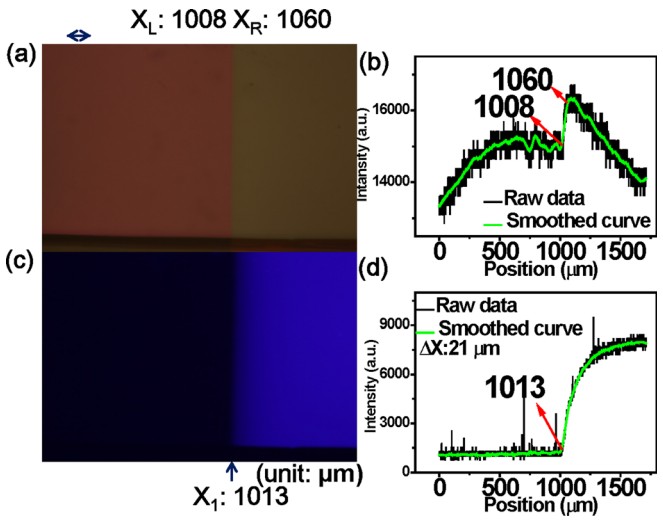

FIG. 30. (a), (b) The bright-field, (c), (d) the dark-field of fixing the thickness of NPB and using chloroform solvent with heating and hot-wind.

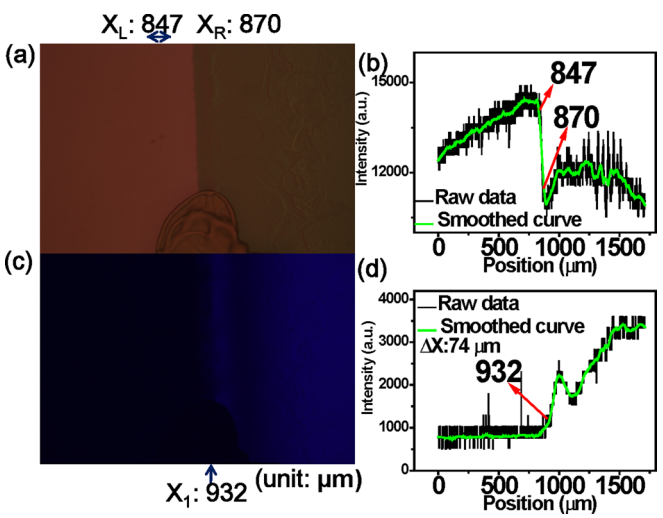

FIG. 31. (a), (b) The bright-field, (c), (d) the dark-field of fixing the thickness of NPB and using chlorobenzene solvent with heating.

TABLE II. The degree of dissolution with different solvent and 20 nm HTL. The samples are made with heating and hot-wind.

Solvent	HTL thickness (nm)	ΔX (μm)
Methanol	20	9
Toluene	20	4
Chloroform	20	21
Chlorobenzene	25	74

same heating conditions. Because the goal of multilayer blade coating is to prevent dissolution by drying rapidly, the slow evaporation of chlorobenzene makes it less suitable for thin layer deposition.

3. No heating or changing solvent

To determine the effects of the key conditions for drying of substrate heating and using hot air, L_2 was blade coated on L_1 with various solvents in the absence of any heating, with L_1 thickness fixed at 20 nm. For the good solvents chloroform and chlorobenzene, the shift of the edge toward the left can be seen in Figs. 32 and 33, which show that the entire L_1 film was dissolved without heating. Because the results above showed that L_1 had to be 20 nm thick to maintain the same edge after chloroform blade coating with heating, these results show collectively that heating is necessary to reduce dissolution. Interestingly, the PL edge did not shift for toluene even without heating (Fig. 34), which may be because toluene dissolves NPB poorly (solubility under 0.5 wt. %). Methanol, as expected, did not shift the PL edge with or without heating (Fig. 35) because NPB is almost insoluble in methanol. Thus, among all the solvents, chloroform appears a good choice for blade coating. Chloroform dissolves a wide range of small molecules reasonably well, and chloroform dissolves to a depth of only 15–20 nm with heating because of its low boiling point. Toluene may attain even smaller dissolution depth than chloroform, but toluene dissolves molecules poorly compared to chloroform. Conversely, chlorobenzene has good solubility but a high

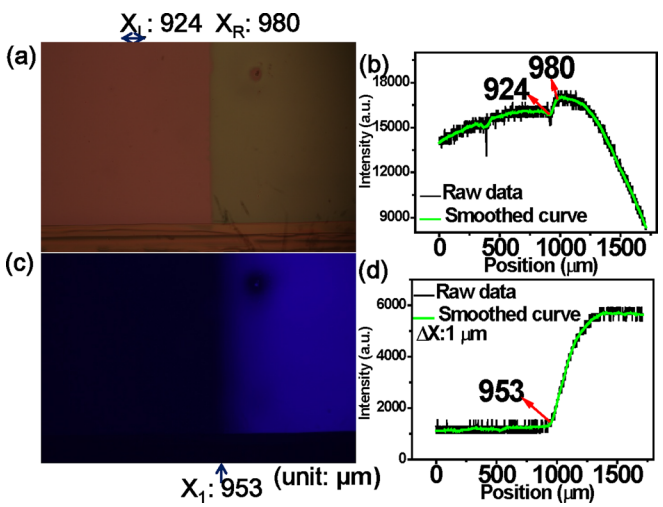

FIG. 32. (a), (b) The bright-field, (c), (d) the dark-field of fixing the thickness of NPB and using chloroform solvent without heating.

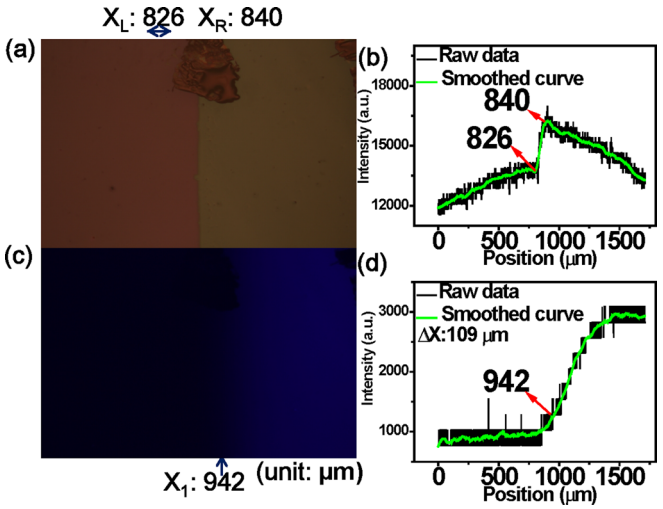

FIG. 33. (a), (b) The bright-field, (c), (d) the dark-field of fixing the thickness of NPB and using chlorobenzene solvent without heating.

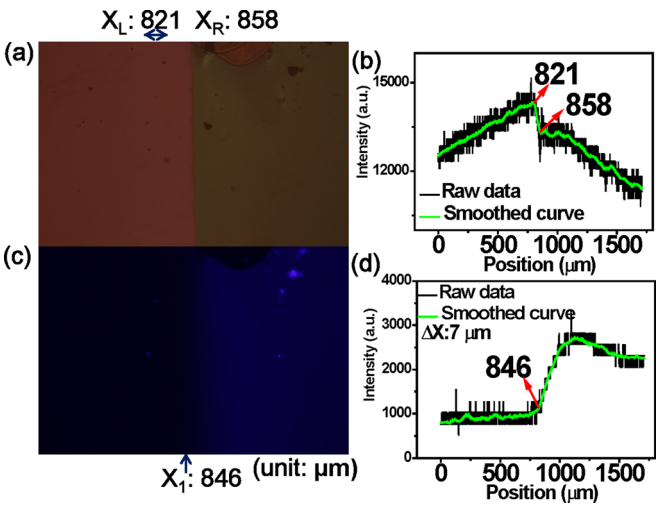

FIG. 34. (a), (b) The bright-field, (c), (d) the dark-field of fixing the thickness of NPB and using toluene solvent without heating.

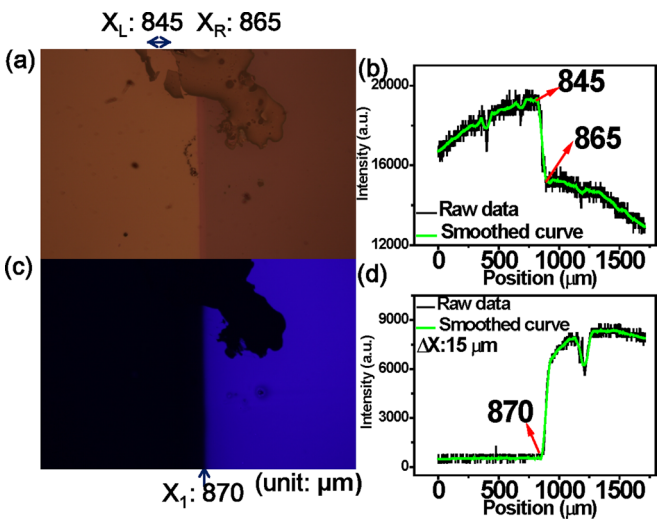

FIG. 35. (a), (b) The bright-field, (c), (d) the dark-field of fixing the thickness of NPB and using pure methanol without heating.

boiling point, and therefore its dissolution depth is above 20 nm even with heating (Table III).

III. OLED DEVICE FABRICATION

Blade coating was conducted using a cylindrical blade with gap between 30 μm and 120 μm. Substrate was heated to 60–100 °C, and hot air from a hair dryer was blown concurrently to ensure that the coated wet film dried rapidly (in approximately two seconds). Dissolution was reduced with such rapid drying. The blade was moved manually at a speed of 30–50 cm/s. The details of the blade coating method have been reported before.[6] The OLED devices were fabricated on glass substrates with a patterned ITO layer. The ITO glass was cleaned in acetone and then exposed to UV-ozone for 15 min. The 50-nm HTL of PEDOT:PSS was spin-coated and annealed at 200 °C for 15 min. The substrates were then placed in a nitrogen glove-box. For white OLEDs, we used 4,4′,4″-tris(carbazol-9-yl) triphenylamine (TCTA) as the HTL. TCTA was dissolved in toluene at 0.5 wt. %, blade spin-coated at 1000–2000 rpm on the PEDOT:PSS layer,[11] and then annealed at 100 °C for 10 min under vacuum (10^{-3} Torr) to remove residual solvent. The resulting TCTA film was 25–35 nm thick. The emission layer (EML) and electron-transport layer (ETL) were deposited subsequently by blade coating on a hot plate without spinning. The hot plate was maintained at 80 °C for rapid drying, and the blade had a gap of 60 μm; 30 μL of the solution was delivered in front of the blade by using a pipette, and the blade was then moved by hand at approximately 60 cm/s to cover the 4 mm^2 active area of the device with the wet film. The emission layer with a thickness of 30–35 nm was next baked for 80 °C for 10 min under nitrogen for white devices. For white OLEDs, we prepared two chlorobenzene solutions separately, using 2,6-bis(3-(9H-carbazol-9-yl)phenyl) pyridine (26DCzppy) and bis (3,5-difluoro-2-(2-pyridyl) phenyl-(2-carboxypyridyl)iridium(III) (FIrpic), 26DCzppy and iridium (III)bis (4-(4-t-butylphenyl) thieno[3,2-c]pyridinato-N,C2′) acetylacetonate (PO-01-TB), 26DCzppy and Bi (1-phenylisoquinoline) (acetylacetonate) iridium(III) (Ir $(piq)_{2acac}$), and 26DCzppy and $Os(fptz)_2(dhpm)$, all at the same weight ratio of 89:11. Before blade coating, the blue and orange (PO-01-TB) solutions were mixed at the prescribed weight ratio of 30:1, the blue, orange (PO-01-TB), and red (Ir $(piq)_{2acac}$) solutions were mixed at the prescribed weight ratio of 30:1:1, and the blue, orange (PO-01-TB), and red ($Os(fptz)_2(dhpm)$) solutions were mixed at the prescribed weight ratio of 30:1:1. The ETL TPBI dissolved in methanol was blade coated on the emission layer at a thickness of 50 nm; 50 μl of the solution was delivered in front of the blade by using a pipette, and the blade was then moved by hand at approximately 30 cm/s to cover the 4 mm^2 active area of the device with the wet film. The shape of the film was sector. The LiF (0.8 nm)/Al (100 nm) cathode was formed by thermal evaporation under vacuum (5×10^{-6} Torr). The completed two-color white OLED had the structure of TCTA/26DCzPPy:PO-01-TB:FIrpic/TPBI, whereas in the three-color OLED, TCTA was used for HTL, and the mixed emitter of PO-01-TB and Ir $(piq)_{2acac}$ or $Os(fptz)2(dhpm)$ was used. The electroluminescence characteristics of the devices were measured using Keithley 2400 and PR650 Spectroscan spectrometers. The Commission internationale de l'éclairage (CIE) coordinates of the white OLEDs were calculated using PR650 software. All measurements were conducted in ambient air after packaging. All small molecules were purchased from Luminescence Technology except for PO-01-TB and $Os(fptz)_2(dhpm)$.

For the orange OLED, we started with device structure of ITO/PEDOT:PSS (50 nm)/NPB (40 nm)/CBP:PO-01-TB = 94:6 (30 nm)/TPBI (30 nm)/LiF (0.8 nm)/Al (100 nm). For green devices, the structure was ITO/PEDOT:PSS (50 nm)/TCTA (30 nm)/26DCzPPy:Ir$(mppy)_3$ = 94:6 (40 nm)/TPBI (40 nm)/LiF (0.8 nm)/Al (100 nm). For simplicity, to avoid dissolution problems with PEDOT:PSS, blade coating was not conducted on a hot plate but on a spinner for the HTL of NPB and TCTA; the blade spin-coating process is shown in Fig. 36. NPB was dissolved in toluene at 0.5 wt. % and blade coated with a gap of 60 μm and spun at 1500 rpm. The film was annealed at 120 °C for 5 min. TCTA was dissolved in toluene at 0.5 wt. %, blade coated with a gap of 60 μm, and then spun at 1500 rpm. The HTL can also be blade coated on a hot plate with hot air and give the same device performance. The film was annealed at 100 °C for 10 min. The EML of the orange OLED was a blend of CBP and PO-01-TB in the weight ratio of 94:6. The blend in chloroform at 0.8 wt. % was blade coated with 60-μm blade gap, and 20 μl or 30 μl of the solution was delivered using a pipette; samples were on a hot plate at 60 °C, which resulted in 20-nm- or 30-nm-thick solid films, and samples were then annealed at 80 °C for 10 min under vacuum. The EML of the green OLED was a blend of 26DCzPPy and tris[2-(p-tolyl)pyridine]iridium(III) (Ir$(mppy)_3$) in the weight

TABLE III. The degree of dissolution with different solvent and 20 nm HTL. The samples are made without heating and hot-wind.

Solvent	HTL thickness (nm)	ΔX (μm)
Methanol	20	15
Toluene	20	7
Chloroform	20	1
Chlorobenzene	25	109

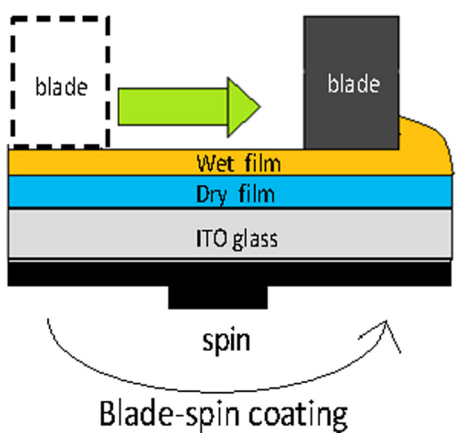

FIG. 36. The blade-spin coating process.

ratio of 94:6. The blend in chloroform at 0.8 wt. % was blade coated with 60-μm blade gap and 40 μl of solution delivered using a pipette; samples were on a hot plate at 60 °C, and they were then annealed at 80 °C for 10 min under vacuum, which resulted in a 45-nm-thick solid film. For the ETL, TPBI of 40 nm was blade coated with a hot-plate temperature of 60 °C, blade gap of 60 μm, and 50 μl of 0.5 wt. % methanol solution. LiF and Al were evaporated under vacuum, and the active area was 4 mm^2. We modulated the thickness of the ETL from 30 nm to 60 nm using the blade-coating process. The 30 nm or 40 nm films were blade coated with 60 μm blade gap, and 30 μl or 40 μl of solution was dripped using a pipette into the gap of the blade. The blade was moved by hand at approximately 100 cm/s. The 50 nm or 60 nm films were blade coated with 60 μm blade gap, and 40 μl of solution was dripped using a pipette 0.5 cm in front of the blade. The blade was moved by hand at approximately 100 cm/s and 150 cm/s. The chemical structures of materials used in OLED fabrication are presented in Fig. 37.

IV. THIN ORANGE OLED

The PL study above showed that the dissolution of the HTL of NPB was between 15 nm and 20 nm using chloroform as the solvent for the second layer. The HTL will therefore be completely removed and mixed with the second layer if it is less than approximately 20 nm thick. Even if the HTL is more than 20 nm thick, its dissolution limits the thickness of the EML. For example, assume that the HTL is 40 nm and the target EML thickness is 20 nm. Although at least 20 nm of HTL will remain intact after the blade coating of the EML, the dissolved 20 nm of HTL may mix completely with the 20 nm of EML. Thus, when the targeted EML is too thin, the partial dissolution of HTL may make the entire EML a mixture with the HTL material and thereby destroy the EML's functions. However, if the targeted EML is well above the dissolution depth, the partial mixing of EML and HTL near the interface may not be a major problem because the device will still have the desired bilayer structure, as shown in Figs. 38(a) and 38(b). To examine the effect of dissolution in blade-coated OLEDs, a series of orange devices with variable EML thicknesses was fabricated using the procedures described above. The orange emitter was PO-01-TB, and 20-nm-, and 30-nm-thick EMLs were compared. The HTL of NPB was fixed at 40 nm. The EML host CBP and the ETL of TPBI were fixed at 30 nm. The device structure is shown in Fig. 39(a), and the results are shown in Figs. 39(b) and 39(c). For comparison (Table IV), the same devices were also fabricated using vacuum evaporation in the same range of EML thickness. When the EML was 30 nm thick, the blade coated devices and evaporated devices performed similarly. However, when the EML was 20 nm thick, the efficiency of the blade-coated device was substantially lower than that of the evaporated devices. This drop in efficiency is expected to be due to the entire mixing of the thin EML with the dissolved part of the HTL (Fig. 38). The current blade coating method therefore cannot be used to deposit films less than 20 nm thick. However, for films above 30 nm, comparison with evaporated devices shows that good multilayer structure is achieved despite partial interface dissolution. In general when the film thickness is well above the dissolution depth the partial inter-layer mixing seems not to be a major problem for the device performance. On the other hand, when the thickness is close to the dissolution depth, the well-defined layers no longer exist, and the efficiency drops significantly as expected. Further improvement of the blade coating technique is required for fabricating multilayer OLEDs less than 20 nm thick. For the orange devices, the different solvents chloroform and chlorobenzene are compared. Although the solubility and film uniformity are both the prerequisites of choosing solvents, the most important feature of our blade coating is rapid-drying. Because chlorobenzene boils at a much higher temperature than chloroform, chlorobenzene dries considerably slower than chloroform. The goal of multi-layer blade coating is to

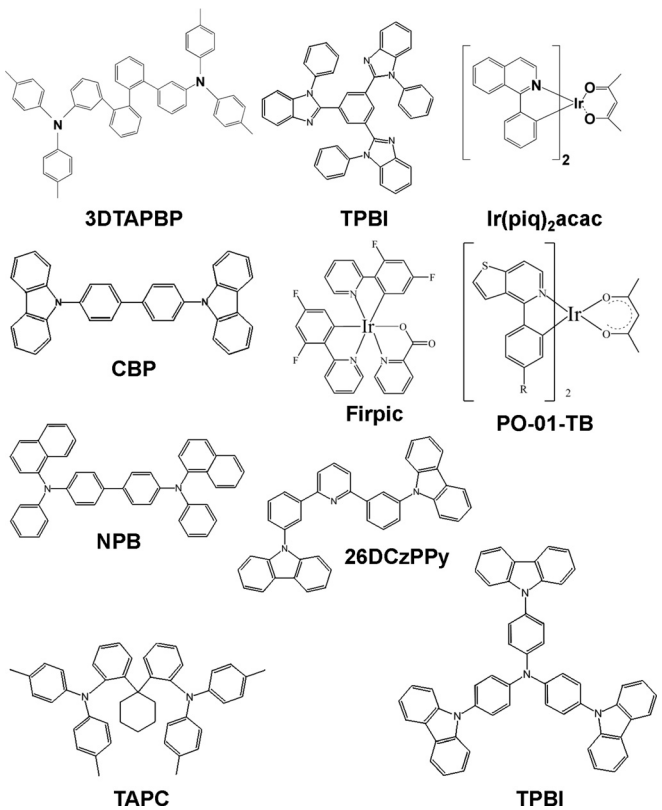

FIG. 37. The chemical structures are used in the OLED fabrications.

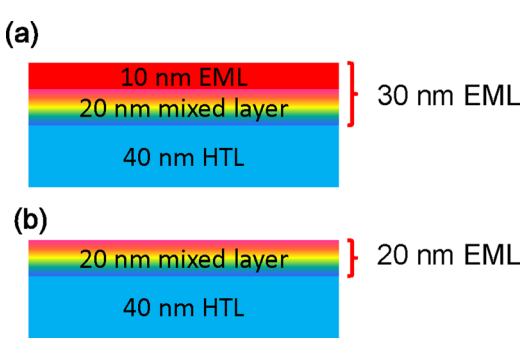

FIG. 38. The bi-layer structure with (a) 30 nm EML and (b) 20 nm EML.

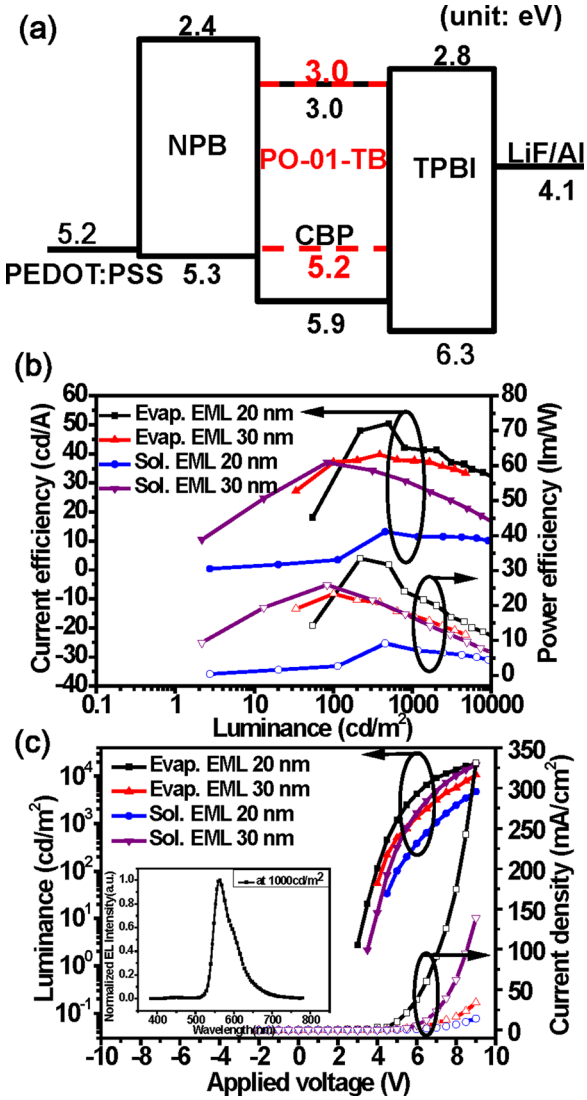

FIG. 39. (a) The device structure of orange OLED. (b) The efficiency versus luminance and (c) the luminance and current density versus voltage with different deposition process and thickness of EML. The inset in (c) shows the normalized EL spectra of the devices.

prevent dissolution by drying rapidly, so slow evaporation of chlorobenzene makes it less suitable for layer deposition. The AFM images and the devices results are shown in Fig. 40. Both of the films give smooth amorphous surface with roughness less than 1 nm. However the surface of

TABLE IV. The characteristic of Orange devices with varying EML thickness ade by evaporation and solution.

Process	Thickness (nm)	Current efficiency (cd/A)	Power efficiency (lm/W)
Evaporation	10	30	20
Evaporation	20	41.3	21.6
Evaporation	30	37.9	16.9
Evaporation	40	…	…
Solution	10	…	…
Solution	20	11.5	7.2
Solution	30	30.8	17.6
Solution	40	26.1	13.6

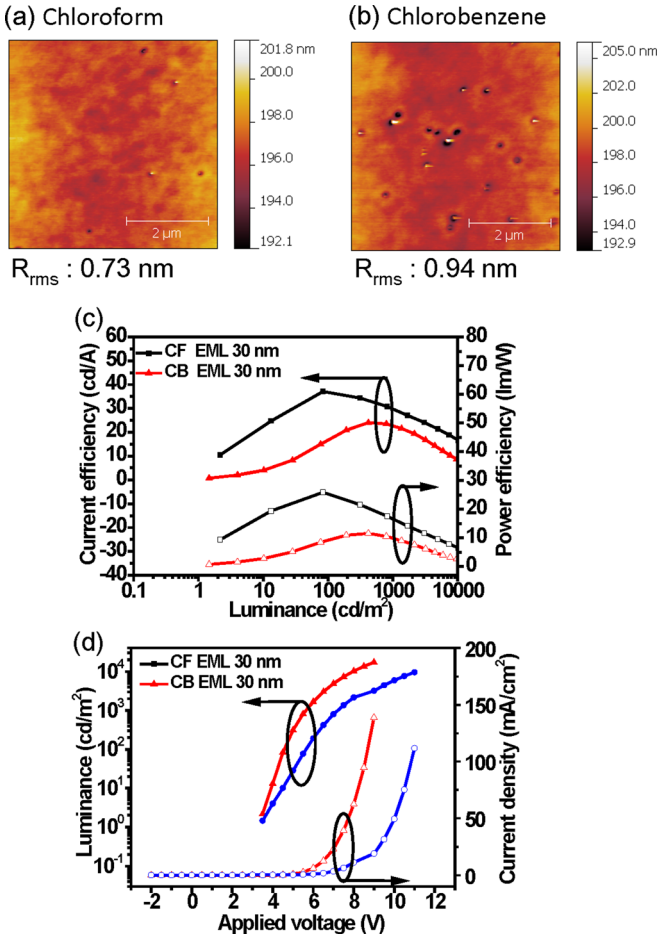

FIG. 40. The AFM rms roughness images of (a) chloroform and (b) chlorobenzene. (c) The efficiency versus luminance and (c) the luminance and current density versus voltage with different solvents of EML.

chlorobenzene film has more dips shown as the black dots. The lower thickness uniformity may be the partial reason for the lower device efficiency by chlorobenzene as shown in Fig. 40.

V. WHITE OLED WITH THICKNESS OVER 20 nm

We next optimized white and green OLEDs by fine-tuning the layer thickness to more the blade coating limit of 20 nm. The device structure and energy levels are shown in Fig. 41(a). TCTA was the HTL, 26DCzPPy was the EML host, and TPBI was the ETL. The EML was doped with the blue emitter FIrpic, orange emitter PO-01-TB, and red emitters $Ir(piq)_{2acac}$ and $Os(fptz)_2(dhpm)$. The weight ratio of 26DCzPPy and the combined emitters was 89:11. The ratio between the emitters FIrpic and P0-01-TB was 30:1. First, TCTA was fixed at 30 nm, TPBI was fixed at 50 nm, and the EML thickness was fixed at 30 nm; the results with this OLED are shown in Figs. 41(b) and 41(c). At the practical luminance of 1000 cd/m^2, the power efficiency was 8.5 lm/W, and current efficiency was 24 cd/A. The optimal power efficiency of 11.6 lm/W was reached at a luminance of 40 cd/m^2. The emissions spectrum and CIE coordinates are shown in Fig. 43.

Because the emission wavelength of PO-01-TB at 560 nm is too short for an ideal white OLED, a common red

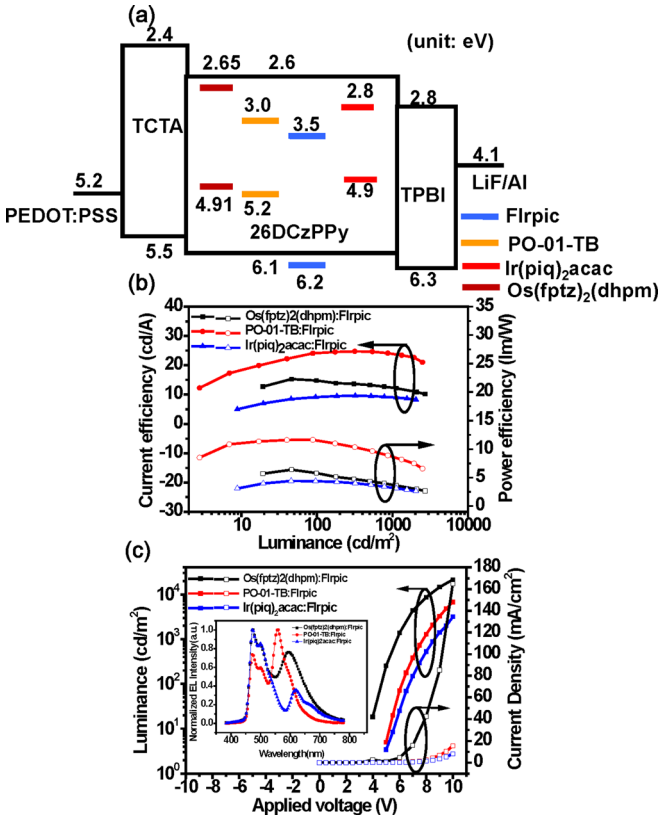

FIG. 41. (a) The device structure of two-color WOLED. (b) The efficiency versus luminance and (c) the luminance and current density versus voltage with different emitters of EML. The inset in (c) shows the normalized EL spectra of the devices.

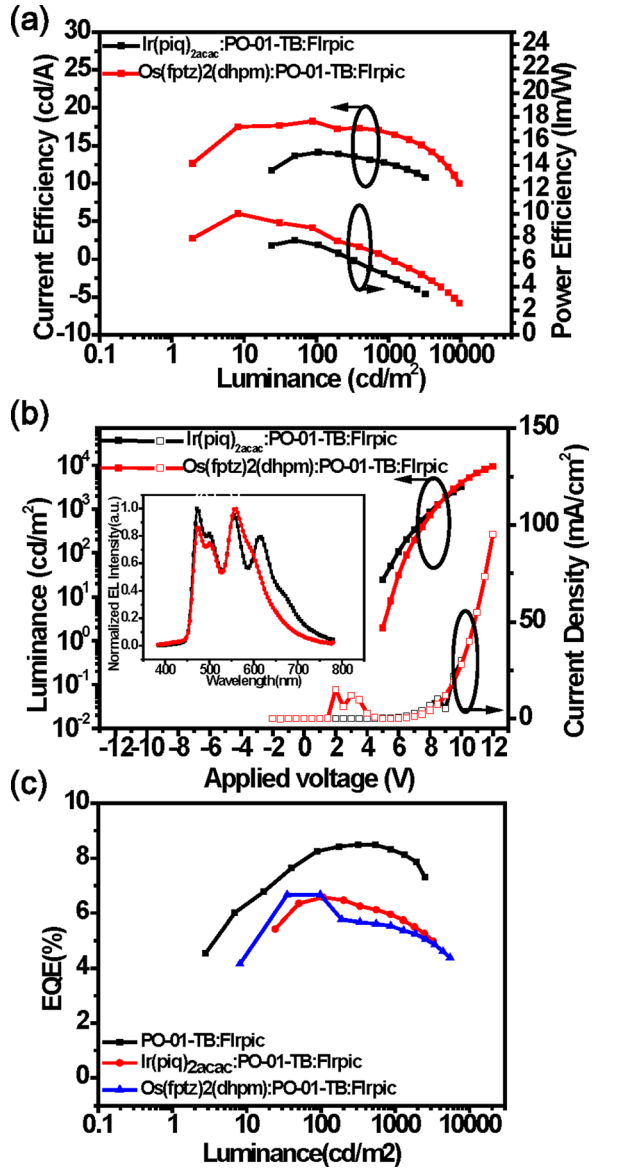

FIG. 42. (a) The efficiency versus luminance and (b) the luminance and current density versus voltage of three-color WOLED with different emitter EML. The inset in (b) shows the normalized EL spectra of the devices. (c) The external quantum efficiency (EQE) of three-color WOLED.

emitter $Ir(piq)_{2acac}$ was added to increase the intensity of long wavelength emission. The ratio of the EML host to all the emitters combined was retained at 89:11, and the ratio among the three emitters, FIrpic, PO-01-TB, and $Ir(piq)_{2acac}$, was 30:1:1. The thickness was fixed at 30 nm for HTL, 30 nm for EML, and 50 nm for ETL. The device structure and energy levels are shown in Fig. 41(a). The performances of the three-color WOLED are shown in Figs. 42(a)–42(c). The power efficiency dropped from 11.6 lm/W for the two-color white OLED to only 4.4 lm/W for the three-color device. However, the two devices had similar external quantum efficiency (EQE), as shown in Fig. 42(c). Thus, the drop in power efficiency was mostly due to the shift of the emission color to the spectral region in which human vision responds more weakly. Three peaks from the three emitters were detected in the emission spectrum shown in Fig. 42(b). Another three-color white OLED was prepared by adding the red emitter $Os(fptz)_2(dhpm)$ to the two-color device, as shown in Fig. 41(a). The ratio among the emitters was retained at 30:1:1, and the device performance and spectrum are shown in Figs. 42(a)–42(c). The white device containing the $Os(fptz)_2(dhpm)$ emitter had power efficiencies of 3.7 lm/W and 12.3 cd/A at 1000 cd/m^2 (Table V), and 6.3 lm/W and 15.2 cd/A at 100 cd/m^2. The CIE coordinates of the three white OLEDs are marked together with the blackbody radiation locus in Fig. 43. Because the EQE values of the three devices were similar, as shown in Fig. 42(c), the one closer to the blackbody radiation locus had lower power efficiency because of the increase in the proportion of red in the spectrum.

VI. GREEN OLED WITH THICKNESS OVER 20 nm

Thickness was tuned for the green OLED as well, and TPBI ETL thickness was found to be critical. The green OLED device structure is shown in Fig. 44(a). The HTL thickness was fixed at 30 nm and EML at 45 nm. For the HTL of TCTA, device performance is shown in Figs. 44(b) and 44(c) for various TPBI thicknesses. At 1000 cd/m^2, the power efficiency and current efficiency were 13.8 lm/W and 38.3 cd/A, respectively. With TAPC as the HTL, efficiency was raised to 23.4 lm/W and 41.9 cd/A at 1000 cd/m^2. The optimal thickness of TPBI was 50 nm with TAPC as the HTL, as shown in Figs. 44(b) and 44(c).

TABLE V. The best characteristic of the Orange devices(NPB(40 nm)/CBP:PO-01-TB(30 nm)/TPBI(30 nm)), the Green device(TAPC(30 nm)/26DCzPPy:Ir(mppy)$_3$(45 nm)/TPBI(50 nm)), and the WOLED(TCTA(30 nm)/EML(35 nm)/TPBI(50 nm)). All the characteristics are at 1000 cd/m^2.

Color	Current efficiency (cd/A)	Power efficiency (lm/W)	CIE (x, y)
Orange	30.8	17.6	(0.51, 0.47)
Green	41.9	23.4	(0.34, 0.61)
2-color white (PO-01-TB:FIrpic)	24	8.5	(0.33, 0.46)
2-color white (Os(fptz)$_2$(dhpm):FIrpic)	12.3	3.7	(0.37, 0.40)
2-color white (Ir(piq)$_{2acac}$:FIrpic)	8.9	3.2	(0.25, 0.37)
3-color white (Ir(piq)$_{2acac}$)	12.5	5	(0.34, 0.41)
3-color white (Os(fptz)$_2$(dhpm))	16.7	6.3	(0.38, 0.44)

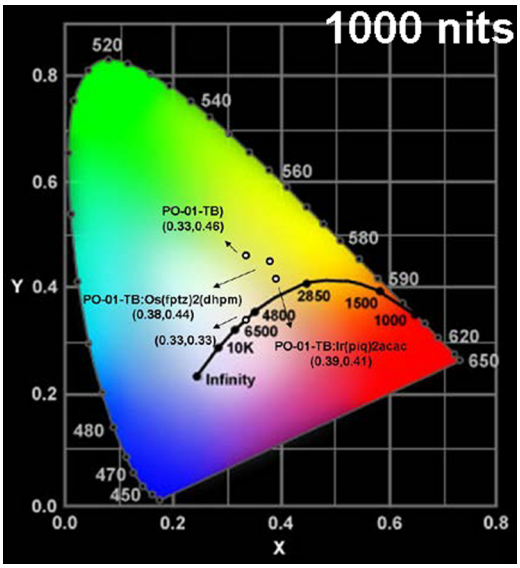

FIG. 43. The CIE coordinates of the two-color and three-color WOLED.

VII. CONCLUSION

Blade coating with rapid drying was applied successfully in fabricating OLEDS, made entirely using chemically unmodified small molecules, for thicknesses above specific processing constraints. Using a new method based on fluorescence imaging, the layer-mixing depth was determined to be approximately 15 nm. Therefore, layer thickness can be tuned only under this constraint. For layers more than 20 nm thick, we fabricated an optimal, all-solution-processed white OLED with high power efficiency (8.5 lm/W) at the practical luminance of 1000 cd/m^2. By combining high performance with the low cost of blade coating, OLED lighting becomes a practical technology. To raise efficiency even more, blade coating techniques have to be improved to allow coating below 20 nm.

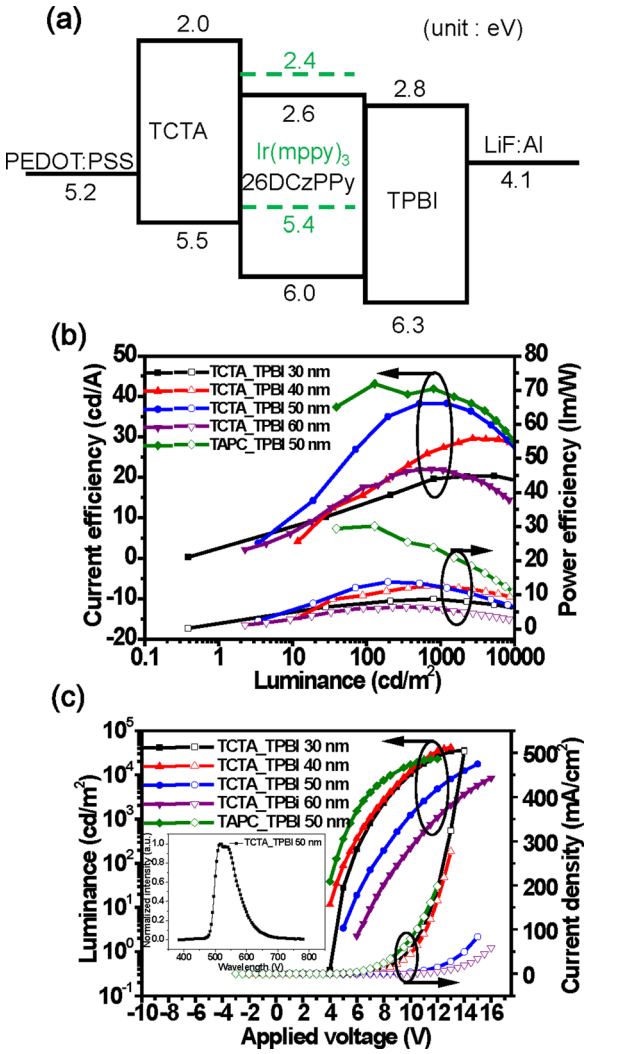

FIG. 44. (a) The device structure of Green OLED. (b) The efficiency versus luminance and (c) the luminance and current density versus voltage with different thickness of ETL. The inset in (c) shows the normalized EL spectra of the devices.

[1]B. Zhang, G. Tan, C. S. Lam, B. Yao, C. L. Ho, L. Liu, Z. Xie, W. Y. Wong, J. Ding, and L. Wang, Adv. Mater. **24**, 1873 (2012).
[2]J. J. Park, T. J. Park, W. S. Jeon, R. Pode, J. Jang, J. H. Kwon, E. S. Yu, and M. Y. Chae, Org. Electron. **10**, 189 (2009).
[3]Y. J. Doh, J. S. Park, W. S. Jeon, R. Pode, and J. H. Kwon, Org. Electron. **13**, 586 (2012).
[4]M. S. Soh, S. A. G. Santamaria, E. L. Williams, M. Pérez-Morales, H. J. Bolink, and A. Sellinger, J. Polym. Sci., Part B: Polym. Phys. **49**, 531 (2011).
[5]S. R. Tseng, H. F. Meng, K. C. Lee, and S. F. Horng, Appl. Phys. Lett. **93**, 153308 (2008).
[6]C. Y. Chen, H. W. Chang, Y. F. Chang, B. J. Chang, Y. S. Lin, P. S. Jian, H. C. Yeh, H. T. Chien, E. C. Chen, Y. C. Chao, H. F. Meng, H. W. Zan, H. W. Lin, S. F. Horng, Y. J. Cheng, F. W. Yen, I. F. Lin, H. Y. Yang, K. J. Huang, and M. R. Tseng, J. Appl. Phys. **110**, 094501 (2011).
[7]H. C. Yeh, H. F. Meng, H. W. Lin, T. C. Chao, M. R. Tseng, and H. W. Zan, Org. Electron. **13**, 914 (2012).
[8]Y. F. Chang, Y. C. Chiu, H. C. Yeh, H. W. Chang, C. Y. Chen, H. F. Meng, H. W. Lin, H. L. Huang, T. C. Chao, M. R. Tseng, H. W. Zan, and S. F. Horng, Org. Electron. **13**, 2149 (2012).
[9]S. J. Su, E. Gonmori, H. Sasabe, and J. Kido, Adv. Mater. **20**, 4189 (2008).
[10]H. Sasabe and J. Kido, Chem. Mater. **23**, 621 (2011).
[11]J. D. You, S. R. Tseng, H. F. Meng, F. W. Yen, I. F. Lin, and S. F. Horng, Org. Electron. **10**, 1610 (2009).